AIAA JOURNAL
Vol. 45, No. 1, January 2007

Noise Reduction Using Smart Panel with Shunt Circuit

Li Jie Zhao,* Heung Soo Kim,† and Jaehwan Kim‡
Inha University, Nam-Ku, Incheon 402-751, Republic of Korea

DOI: 10.2514/1.20077

Piezoelectric smart panels featuring shunt damping are designed and tested for broadband noise reduction. Electrical admittance is introduced to represent electromechanical coupling of piezoelectric structures. Admittance is used to predict the performance of piezoelectric shunt damping. The location, size, and rotational angle of piezoceramic patches on the host panel are optimized by taking the admittance as a cost function and by using the Taguchi method. The admittance is calculated by finite element method in the design stage and experimentally verified after the optimal configuration is found. Shunt performance of the smart panel is realized by vibration reduction in frequency domain. To illuminate the effect of noise reduction in the shunt system, a standard test setup according to SAE J1400 is used to measure the transmission loss and sound pressure distribution for the smart panel. In this paper, a broadband shunt technique for increasing transmission loss is experimentally investigated.

I. Introduction

NOISE radiating from vibrating structures is a vital problem in the field of engineering and many efforts have been conducted to reduce radiating noise. The study of smart structures in the past decade offers great potential in reducing vibration and acoustic emission [1–3]. Piezoelectric materials are employed as both actuators and sensors in the development of smart structures by taking advantage of direct and converse piezoelectric effects. Generally, an active control system has been extensively used to decrease the noise radiation from the vibrating structure. Sun et al. studied two distributed piezoelectric actuators to reduce the vibration and noise of the structure [4]. Shields et al. applied a piezoelectric damping to composite structure for active control of the vibration of the structure [5]. Varadan et al. also demonstrated how to control the sound radiation and noise of the main plate [6,7]. Lecce et al. illuminated active vibration control in a vehicle by using piezoelectric sensors and actuators [8]. Lee et al. demonstrated noise reduction using passive and active hybrid panels [9]. However, the active control technique has drawbacks due to the increased complexity of the controller and expensive system. In contrast, passive control does not bring any of the complexity and expensiveness brought from active control. For passive control, it is impractical for low frequency because an increasing amount of materials is required. To compensate for the disadvantages of active control and passive control, a passive shunt damping technique using piezoceramic patches with a shunt circuit has been investigated, because a passive piezoelectric shunt system is simple, compact, and low cost compared with active damping technology and also has advantages of broad bandwidth in vibration reduction and robust temperature characteristics compared with traditional passive damping technology using viscoelastic materials [10–12].

Piezoelectric shunt damping is a technology in which the mechanical energy in structure is transferred to electrical energy through piezoceramic patches bonded on the structure and transferred electrical energy is dissipated by heat through the resistor in a shunt circuit attached to the structure [11,12]. Generally, piezoelectric shunt systems consist of a host plate on which piezoceramic patches are bonded and an electric shunt circuit is networked to the piezoceramic patches. It is important to design an effective piezoelectric structure, termed as a smart panel, and proper shunt circuit for the high performance of a piezoelectric shunt system. To dissipate external vibration or acoustical energy efficiently, the piezoelectric structure must be constructed to generate more charges on the surface of piezoceramic patches bonded on the host structure, and the shunt circuit must be tuned to suppress and to dissipate the vibration energy at resonance into heat. Most researches have been concentrated on the piezoelectric shunt circuit such as development of efficient shunt circuit, design of multimode shunt circuit, and optimization of circuit parameters [13–20]. Recently, several studies reported that the configuration of piezoceramic patches was important for designated target frequency and mode shape [21–23]. However, only mechanical characteristics of piezoelectric structures were considered. Based on this study, it is difficult to design a piezoelectric structure in real application and to predict the performance of the piezoelectric shunt system. To overcome this, electromechanical characteristics of the piezoelectric structure need to be considered.

In this paper, admittance is introduced to represent electromechanical coupling of the piezoelectric structure. The relation between admittance and dissipated energy in the shunt circuit is investigated first and then admittance is used as a performance index for optimal design of a smart panel. The Taguchi method is used to obtain optimal configuration of a smart panel. Admittance is used as a cost function in the optimal design process. Full three-dimensional finite element models are analyzed to simulate vibration modes of a smart panel and to obtain admittance of the system. Vibration reduction of a smart panel is measured to study the improvement of shunt performance. In addition, noise reduction with a shunt circuit is investigated by transmission loss and sound pressure distribution of piezoelectric structures. Two smart panels are compared through numerical analysis and experiment to show the correlation of the results for the design.

II. Optimization of Smart Panel Using Admittance

The smart panel is configured as shown in Fig. 1. A piezoceramic patch is bonded on the surface of the host structure and networked to the shunt circuit. Mechanical energy of vibration is transferred to electrical energy at the piezoceramic patch and the transferred electrical energy is dissipated at the shunt circuit.

A Admittance and Dissipated Energy

Admittance of piezoelectric structure is known as a representative parameter of electromechanical couplings in a piezoelectric shunt

Received 15 September 2005; revision received 9 October 2006; accepted for publication 10 October 2006.

*Graduate Research Associate, Department of Mechanical Engineering, 253 YongHyun-Dong; darwinzhao@hotmail.com.

†Research Professor, Department of Mechanical Engineering, 253 YongHyun-Dong; Corresponding Author, heungsookim@inha.ac.kr. Member AIAA.

‡Professor, Department of Mechanical Engineering, 253 YongHyun-Dong; jaehwan@inha.ac.kr. Member AIAA.

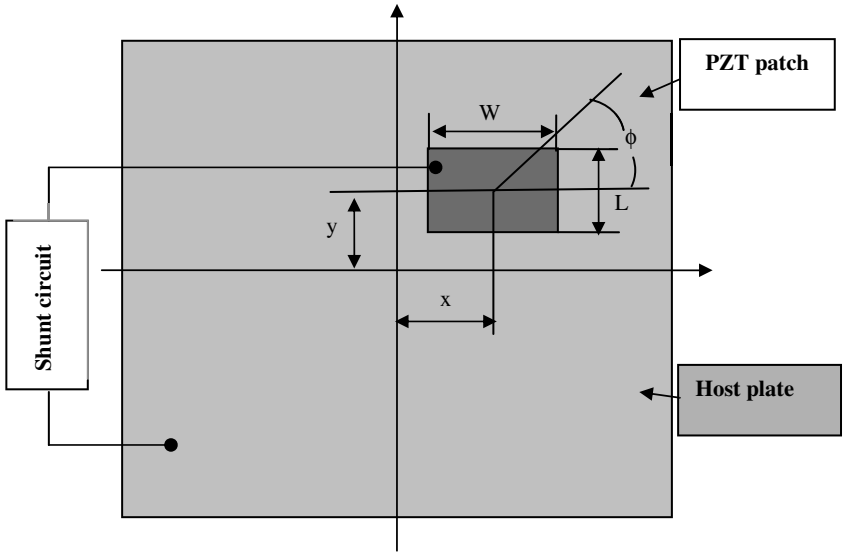

Fig. 1 Schematic of the smart panel.

system [24]. Admittance analysis, that is the record of the spectrum of electrical admittance of the compound resonator as a function of the exciting frequency, has changed the focus from the physical behavior of the system to its electrical opponents. When the exciting frequency of the piezoelectric structure is much lower than the natural frequency of piezoelectric materials, an equivalent electric model of a piezoelectric structure can be obtained as shown in Fig. 2. In the equivalent electric model, C_0 is capacitance of piezoelectric material and L_1, C_1, and R_1 represent equivalent mass, compliance, and damping of the host structure, respectively. If the shunt circuit is assumed as a serial resonant circuit, impedances of the equivalent electric model are expressed as follows [25].

$$Z_1(s) = m_1 s + \frac{k_1}{s} + c_1 = j\omega L_1 + \frac{1}{j\omega C_1} + R_1 \tag{1}$$

$$Z_2(s) = \frac{k_0}{s} = \frac{1}{j\omega C_0} \tag{2}$$

$$Z_3(s) = j\omega L + R \tag{3}$$

where Z_1 is the impedance of the host structure, $Z_2$is the impedance of the piezoelectric patch, and Z_3 is the impedance of the shunt circuit. Because the total impedance of the system can be calculated as

$$Z = Z_1 + \frac{Z_2 Z_3}{Z_2 + Z_3} \tag{4}$$

The admittance of the piezoelectric patch is the reciprocal of its impedance as follows.

$$|Y| = \frac{1}{|Z|} \tag{5}$$

The induced power can be defined in terms of the equivalent electrical circuit according to Fig. 2. The induced power of the system under external excitation is

$$P_{\text{in}} = \frac{1}{2}|V \cdot i_1^*| = \frac{1}{2}\left|\frac{i}{Y} \cdot i_1^*\right| = \frac{1}{2}\left|\frac{1}{Y}\right| \cdot |i_1|^2 \tag{6}$$

where i_1^* is the complex conjugate of the current i_1.

In open circuit state, i.e., $Z_3 = \infty$, total current of a piezoelectric patch generated under external excitation i_O is given as follows.

$$i_O = \frac{V_O}{(Z_1 + Z_2)} = V_O \cdot Y_{12} \tag{7}$$

where $Y_{12} = (Z_1 + Z_2)^{-1}$ represents admittance of the piezoelectric structure in open circuit. The voltage V_O represents voltage of a piezoelectric patch in open circuit. When the shunt circuit is connected to the structure, i.e., $Z_3 \neq \infty \neq 0$, the total current of the piezoelectric shunt system can be expressed as follows.

$$i_1 = i_2 + i_3 = V_3 \cdot \left(\frac{Z_2 + Z_3}{Z_2 \cdot Z_3}\right) \tag{8}$$

If the same external excitation is applied to the smart panel before and after connecting the shunt circuit, total current generated in each system is the same and can be expressed as $i_O = i_1$. From Eqs. (7) and (8), voltage applied to the shunt circuit V_3 and current flowing in the shunt circuit i_3 are expressed as follows.

$$V_3 = V_O \cdot Y_{12} \cdot \frac{Z_2 \cdot Z_3}{Z_2 + Z_3} \tag{9}$$

$$i_3 = \frac{Z_2}{Z_2 + Z_3} \cdot i_O \tag{10}$$

Meanwhile, the dissipated power can be described as

$$\begin{aligned} P_D &= \frac{1}{2}|V_2 \cdot i_3^*| = \frac{1}{2}|[\text{Re}(Z_3) \cdot i_3] \cdot i_3^*| = \frac{1}{2}\,\text{Re}(Z_3) \cdot |i_3|^2 \\ &= \frac{1}{2}\,\text{Re}(Z_3) \cdot \left|\frac{Z_2}{Z_2 + Z_3}\right|^2 \cdot |i_O|^2 \\ &= \frac{1}{2}\,\text{Re}(Z_3) \cdot \left|\frac{Z_2}{Z_2 + Z_3}\right|^2 \cdot |V_O|^2 \cdot |Y_{12}|^2 \end{aligned} \tag{11}$$

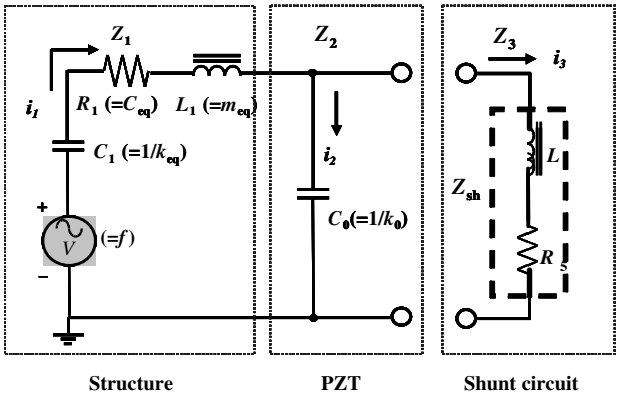

Fig. 2 Equivalent circuit of the smart panel.

From Eq. (11), the dissipated power is proportional to the quadratic form of electromechanical characteristic values ($|Y_{12}|^2$) of piezoelectric structure in an open circuit. If the voltage V_O is applied, admittance can be measured and it is an independent constant. On the other hand, the dissipated power is only a function of admittance of piezoelectric structure in an open circuit. Therefore, the reduction of vibration in the piezoelectric shunt system is dependent on admittance of piezoelectric structure and admittance can be regarded as a performance index in designing a smart panel.

B. Analysis of Admittance

Finite element analysis is an effective method for the analysis of structural response, because it is applicable to arbitrary shapes and geometries. Admittance of piezoelectric structure is analyzed by the electromechanical impedance model [26] or the finite element method [27–29]. Admittance consists of real part, conductance, and imaginary part, susceptance. The magnitude of electromechanical coupling is represented by conductance. After finite element discretization, equations of motion for the piezoelectric structure in matrix form are expressed as follows [30].

$$\begin{Bmatrix} [M] & [0] \\ [0] & [0] \end{Bmatrix} \begin{Bmatrix} [\ddot{u}] \\ [\ddot{\phi}] \end{Bmatrix} + \begin{Bmatrix} [D] & [0] \\ [0] & [0] \end{Bmatrix} \begin{Bmatrix} [\dot{u}] \\ [\dot{\phi}] \end{Bmatrix} + \begin{Bmatrix} [K] & [K_{u\phi}] \\ [K_{u\phi}]^t & [K_\phi] \end{Bmatrix} \begin{Bmatrix} [u] \\ [\phi] \end{Bmatrix} = \begin{Bmatrix} [F] \\ [Q] \end{Bmatrix} \tag{12}$$

$$|Y| = \left| \frac{i}{V} \right|, \qquad i = j\omega \sum_i Q_i \tag{13}$$

$$Y = G + jB \tag{14}$$

where

$[F], [u]$= vector of nodal structural forces and displacements

$[M], [D], [K]$= structural mass, damping, and stiffness matrix

$[Q], [\phi]$= vector of nodal electrical charges and potential

$[K_{u\phi}], [K_\phi]$= piezoelectric coupling and dielectric conductivity matrix

t= transposed

i, V= current and voltage

Y, G, B= admittance, conductance, and susceptance

Q_i= the point charge of the ith node on the electrode

To formulate the preceding equation, commercial finite element code ANSYS is used. From the preceding equations, mode shapes and natural frequencies of the smart panel are extracted through modal analysis and admittances of the piezoceramic patch are obtained through harmonic analysis.

C. Optimizing the Smart Panel

Optimal design of piezoelectric structure is proposed based on admittance at resonance. The basic configuration of the smart panel is shown in Fig. 1. The dimension of the host aluminum plate is $350 \times 350 \times 1.5$ mm. Three different design parameters of the piezoelectric patch are considered, such as location, size, and rotational angle of the piezoceramic patch. The Taguchi method was applied in the optimizing process. The Taguchi method is generally employed as a tool for systematic experimental design. The key of the Taguchi method is the use of parameter design, which is the ability to design a product or a process to be robust to various environmental factors. It can replace full factorial design using partial factorial design. The method ascribes to the approach that the lowest loss to society represents the product with the highest quality [31]. If the parameters and levels have been specified, the partial trials, instead of the whole amount of trials, can be determined by means of the orthogonal array determined by the Taguchi method (see Tables 1 and 2). Admittances of different configurations of the piezoelectric patch on the host plate were calculated by ANSYS to be the cost function in optimization. The boundary conditions of the host plate were all four-sided clamped and the piezoceramic patch was considered as perfectly bonded to the host structure in the finite element analysis.

Table 1 Control factors

Factors		Levels		
		1	2	3
ϕ	rotation angle, deg	0	45	——
x	x-coordinate, mm	0	25	50
y	y-coordinate, mm	0	25	50
L	length, mm	50	75	100
W	width, mm	50	75	100

Using orthogonal array, 18 configurations of the piezoceramic patch on the surface of the host structure are found (Table 2) and the result provides an optimal configuration of the patch on the host structure. One can obtain S/N ratio for each configuration by means of the admittances and the optimal result from the main effect plot of S/N ratio (Fig. 3). According to "larger is better" in the process of optimization, the optimal result is the (1 1 1 3 3) case, that is the piezoceramic patch will lie in the center of the host structure and the size is 100×100 mm, whereas the rotation angle of the piezoceramic patch on the host plate is 0 deg. From the result using the Taguchi method, although the optimal model is not included in the trials, it can be extracted through the Taguchi optimization.

D. Comparison of Initial and Optimal Model

Two models, initial and optimal, were investigated to correlate the numerical and experimental results. From the numerical analysis, the optimal model was obtained. The size of the piezoceramic patch obtained from optimal design is $100 \times 100 \times 0.5$ mm. The initial model was selected to compare them with each other. The dimension of initial model is $100 \times 50 \times 0.5$ mm. The schematic of the configurations are shown in Fig. 4. Mode shapes and corresponding natural frequencies of the optimal model are shown in Fig. 5. Mode shapes of the initial model are the same as those of the optimal model. The corresponding natural frequencies shift up a little due to the mass and piezoelectric softening effects.

III. Setups of Experimental System

To correlate the results of numerical analysis, three different experimental systems were constructed. The purpose of the experiments is to examine the numerical admittances, the vibration

Table 2 Orthogonal array table of L_{18}

Trial no.	Column no.				
	1	2	3	4	5
1	1	1	1	1	1
2	1	2	2	2	2
3	1	3	3	3	3
4	1	2	1	1	2
5	1	2	2	2	2
6	1	2	3	3	1
7	1	3	1	2	1
8	1	3	2	1	2
9	1	3	3	1	3
10	2	1	1	3	3
11	2	1	2	1	1
12	2	1	3	2	2
13	2	2	1	2	3
14	2	2	2	3	1
15	2	2	3	1	2
16	2	3	1	3	2
17	2	3	2	1	3
18	2	3	3	2	1

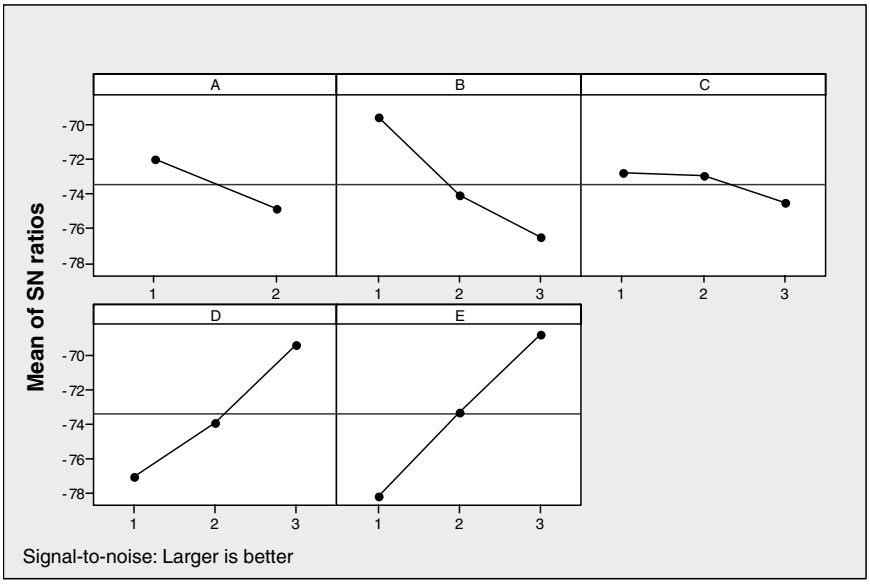

Fig. 3 Main effect of means of SN ratio.

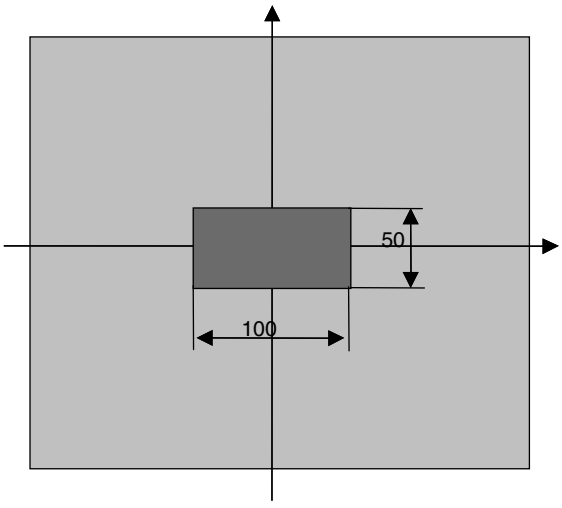

a) Initial configuration

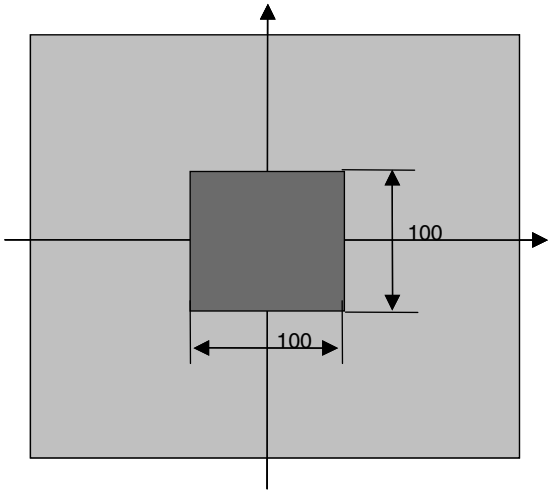

b) Optimal configuration

Fig. 4 Initial and optimal configuration of smart panel.

reduction, as well as noise reduction, after switching on/off the shunt circuits to verify the performance of the piezoelectric shunt.

A. Admittance of Smart Panel

The admittances for the initial and the optimal model were measured by the impedance analyzer (HP4192A). The experimental setup is presented in Fig. 6. The admittance value was measured at open circuit state. According to the poling direction, the positive electrode of the impedance analyzer was connected to the top surface of the piezoceramic patch that is away from the host plate. The negative electrode of the impedance analyzer was connected to the host plate.

B. Vibration Reduction of Smart Panel

Actually, the resonance of the smart panel will be shifted a little in real application. Therefore, it is very important to find the optimal inductance and resistance for the shunt circuit. The purpose of the tuning process is to find the resonance in the real application for the best performance of shunt damping. The setup for this purpose is shown in Fig. 7. To excite the smart panel, actuating the piezoceramic patch, the dimension of which is $50 \times 50 \times 0.5$ mm, is bonded on the center of the smart panel. An accelerometer (charge accelerometer type 4374, B&K) is attached on the surface of the piezoceramic patch for shunt damping on the other side of the smart panel. In the shunt circuit, the synthetic inductor was used as shown in Fig. 8. Tuning the value of resistor R_2, the real resonance of the shunt circuit can be found. Tuning the value of load resistor R_5, the optimal damping is achieved. The testing devices include portable FFT analyzer CF-3200 manufactured by ONO SAKK company.

C. Acoustic Test for Smart Panel

To investigate noise reduction, transmission loss and sound pressure distribution are investigated. Transmission loss is the accumulated decrease in acoustic intensity as an acoustic pressure wave propagates outwards from a source. The term transmission loss (TL), or more commonly sound reduction index, are used to evaluate the reduction in sound level resulting from transmission through the plates. The sound pressure distribution is used to correlate the results of modal analysis in the finite element code and shunt performance of the smart panel using a shunt circuit. To test the performance of the smart panel with shunt circuit about noise reduction and transmission loss, as well as sound distribution test, a standard facility was built according to SAE J1400. The schematics are shown in Figs. 9 and 10. The transmission loss test facility includes two adjacent rooms, a

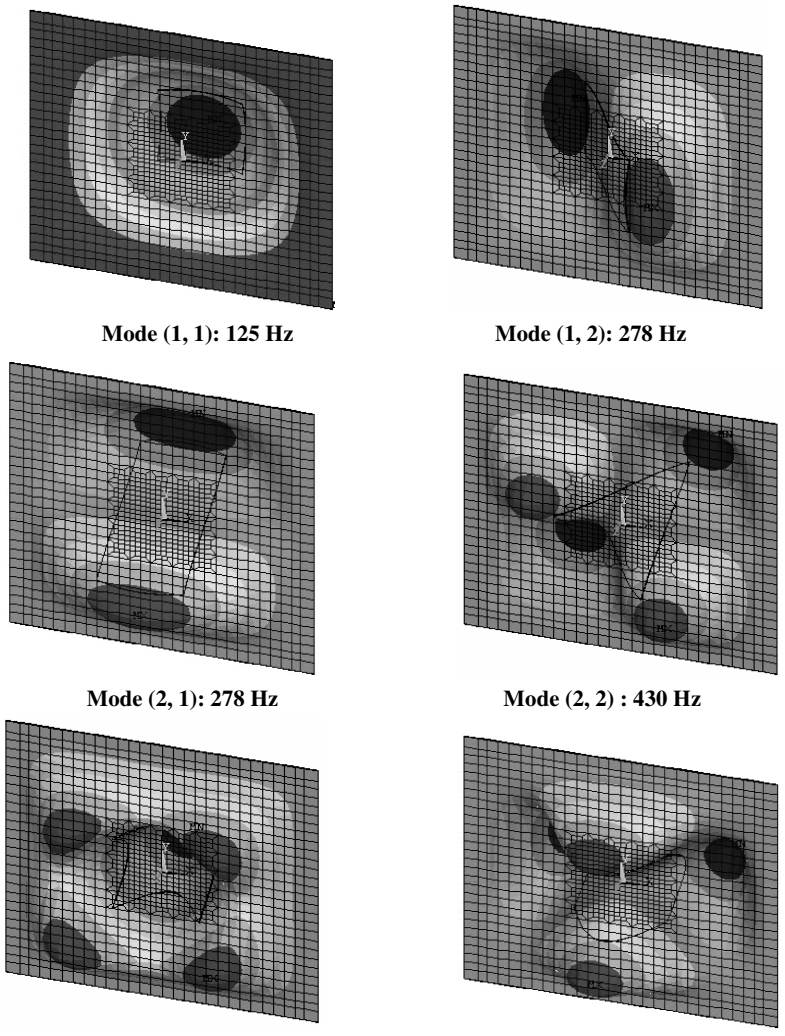

Fig. 5 Mode shapes and natural frequencies of optimal model.

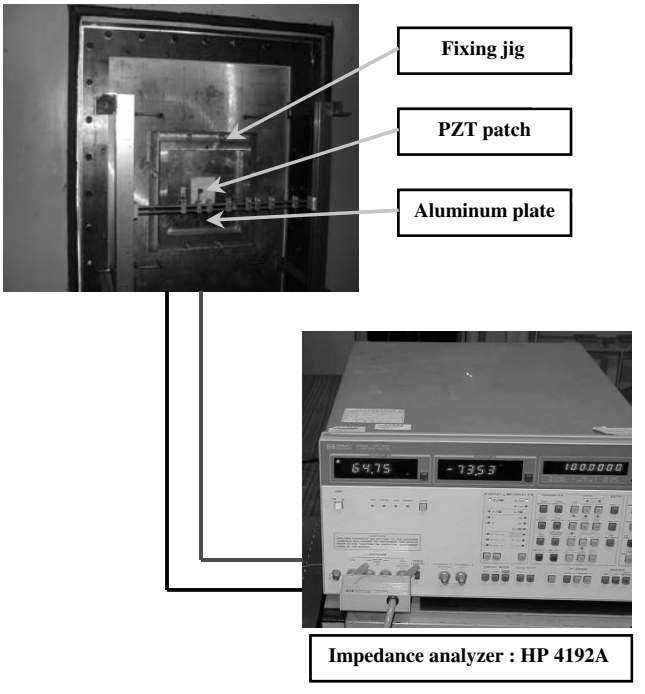

Fig. 6 Experimental apparatus for admittance measurement.

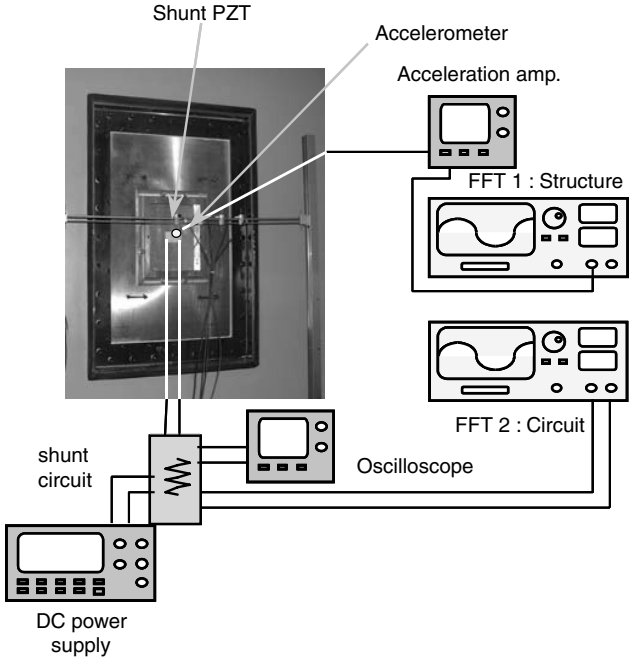

Fig. 7 Experimental setup for piezoelectric shunt damping.

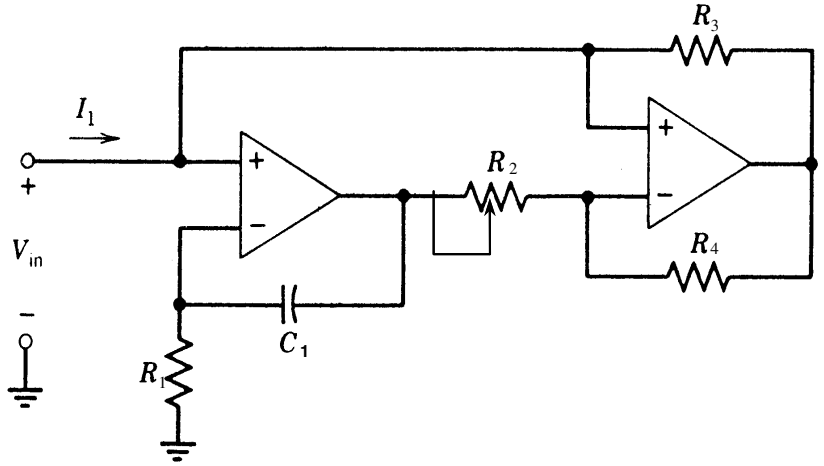

Fig. 8 A schematic diagram of synthetic inductor.

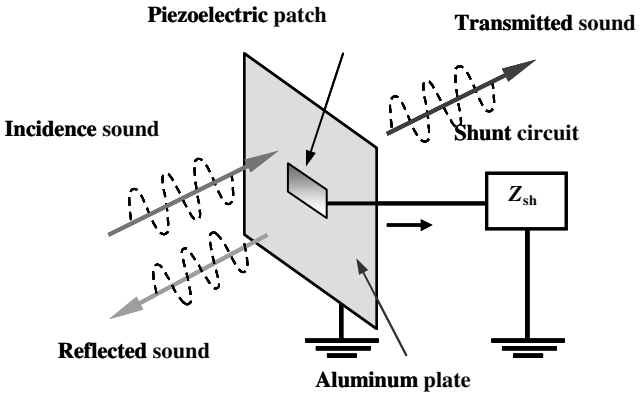

Fig. 9 Schematic diagram of piezoelectric structure.

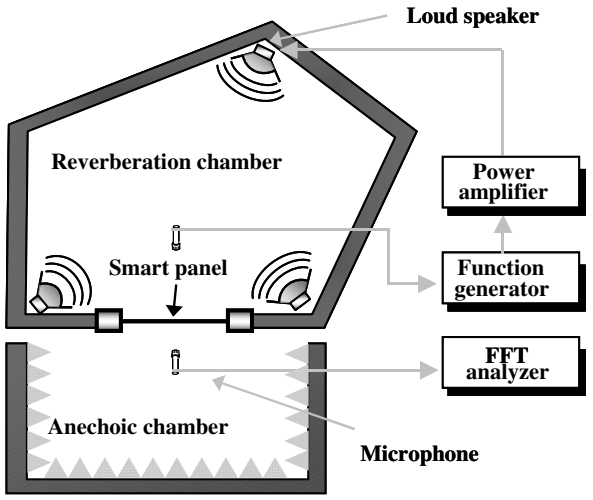

Fig. 10 A schematic diagram for TL measurement.

reverberation room and a semi-anechoic reception room. A test window is located between the two rooms where smart panels are clamped for testing. Noise or plane wave is generated through the loudspeakers in the reverberation room, and the amount of sound reflected and transmitted through the window is measured through microphones in the reverberation room and the reception room. Initial tests were operated with this window to calibrate the data acquisition program that measures the noise reduction and calculates the panel transmission loss. Once the test setup was calibrated, transmission loss was measured for three different test panels: 1) a standard test panel for the constant correction factor, 2) initial model

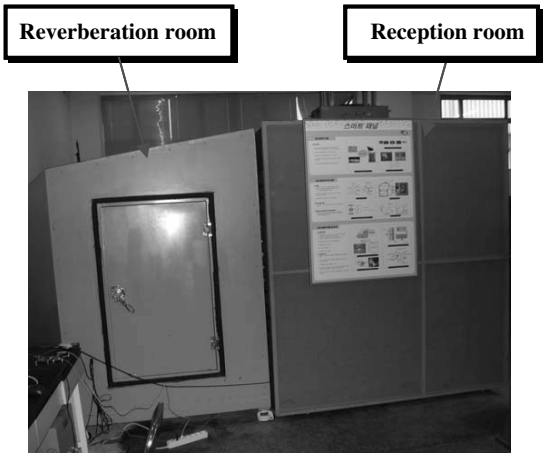

Fig. 11 Photograph of reverberation and reception room.

of the smart panel, and 3) optimal model of the smart panel. The real setup is presented in Fig. 11. The testing devices include a sound signal amplifier (Inter VI PA-4000 public address amplifier) to magnify the source signal and 3560-B-040 FFT analyzer made by B&K company.

IV. Results and Discussions

After the numerical analysis and optimizing process, the initial and optimal model are selected to correlate the numerical and experimental results. Four experiments were conducted.

A. Correlation of Admittance Between Numerical and Experimental Results

Using the modal analysis solver in the commercial finite element code, the natural frequencies of the initial model and optimal model are computed. Referring to the experiment mentioned in Sec. III.A, the natural frequencies were extracted from the measurement of admittance. Comparisons of the strong radiation mode at different natural frequencies for the initial model and optimal model, which are mode (1, 1) and mode $(1,3)$ + mode $(3,1)$, are shown in Table 3. Using harmonic analysis in the commercial finite element code, the admittances of the two models were computed and the experimental values were obtained by means of Sec. III.A. The comparisons are presented in Figs. 12 and 13. Admittance is a complex value and consists of the real part, conductance, as well as the imaginary part, susceptance. Although the magnitude of numerically obtained susceptance deviates a lot from experimentally obtained ones, conductance and natural frequencies correlate well. It

Table 3 Comparisons of natural frequencies for initial and optimal model

Model	Finite element method	Experiment
	frequency, Hz	frequency, Hz
100 × 50 mm	129	125
	503	496
100 × 100 mm	125	122
	505	512

certifies the results are reasonable. In the meantime, the optimal model can generate more charges on the surface of the smart panel than the initial model according to the figures. It represents that the optimal model can dissipate more vibration energy than the initial model.

B. Shunt Damping

After modal analysis, mode (1, 1) and mode $(1, 3)$ + mode $(3, 1)$ were selected as the target modes in the shunt circuit which need tuning to find optimal shunt damping because they were strong radiation modes. Figures 14 and 15 show the experimental results for the initial and optimal model under switching on/off shunt damping circuit. Four different conditions of the smart panel, such as open circuit, short circuit, underdamping, and optimal damping, were tested separately. According to the resonance at open circuit state, the R_2 (Fig. 8) was tuned to match the resonance and then the load resistor R_5 (Fig. 2) was tuned for optimal damping. For the initial

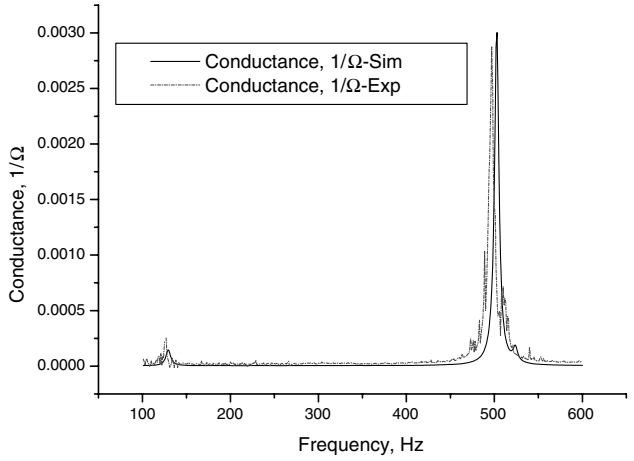

a) Conductance

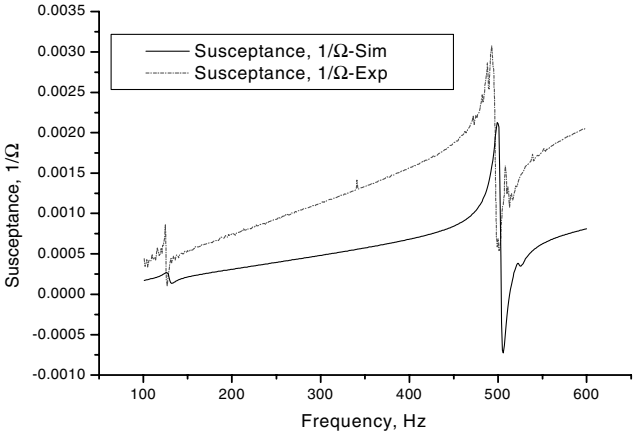

b) Susceptance

Fig. 12 Comparison of experimental and numerical admittance of initial model.

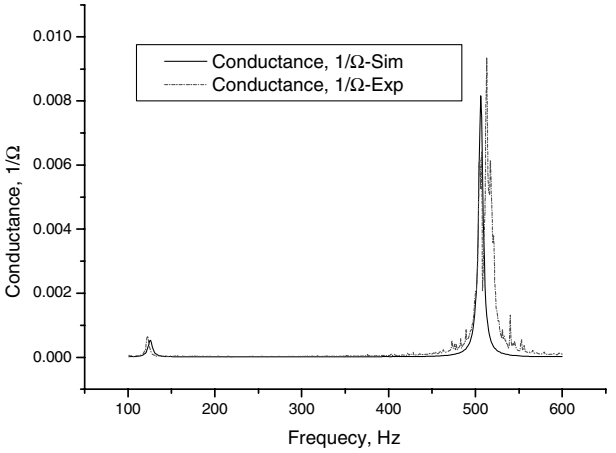

a) Conductance

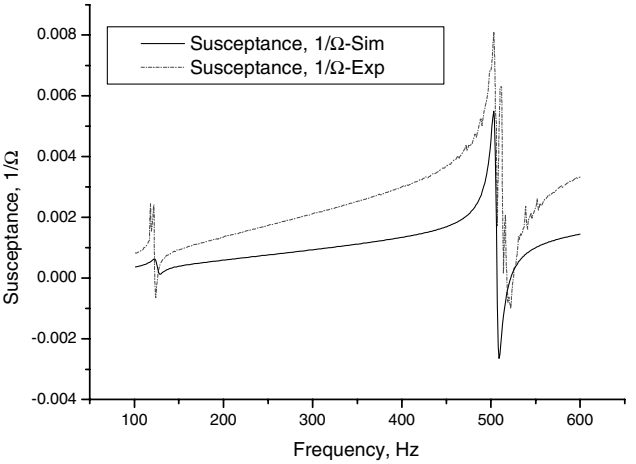

b) Susceptance

Fig. 13 Comparison of experimental and numerical admittance of optimal model.

model, the tested results are observed according to four testing conditions. Figure 14a shows the frequency response function (FRF) of mode (1, 1). At open and short circuit with shunt off, the resonance is shifted a little due to piezoelectric softening effect. After tuning $R_2 = 120\ \Omega$ with shunt on, mode (1, 1) is matched when the load resistor is $R_5 = 0\ \Omega$, which represents the underdamping state. Tuning the load resistor $R_5 = 696\ \Omega$ through fixing R_2, the optimal damping can be observed and 16 dB vibration reduction is achieved. For mode $(1, 3)$ + mode $(3, 1)$, it shows the same trends and $R_2 = 200\ \Omega$, $R_5 = 0\ \Omega$specified the underdamping state, as well as $R_5 = 164\ \Omega$ specified the optimal damping. The 18 dB vibration reduction is achieved (Fig. 14b). By means of the same testing process, the testing results can be found from the optimal model. Figure 15a shows the FRF of mode (1, 1). The optimal damping is $R_2 = 240\ \Omega$ and $R_5 = 463\ \Omega$. The 20 dB vibration reduction is achieved in mode (1, 1). Figure 15b shows the FRF of mode $(1, 3)$ + mode $(3, 1)$, the optimal damping is $R_2 = 418\ \Omega$ and $R_5 = 100\ \Omega$. The 22 dB vibration reduction is achieved for mode $(1, 3)$ + mode $(3, 1)$. Consequently, from the optimal tuning process, better shunt damping effects are observed. The optimal model proposed better damping performance compared to the initial model (Table 4). The shunt performance was improved 25% at mode (1, 1) and 22% at mode $(1, 3)$ + mode $(3, 1)$.

C. Transmission Loss

Three different test panels were used for the transmission loss tests referring to the setup in Sec. III.C. Transmission loss is determined as follows [32].

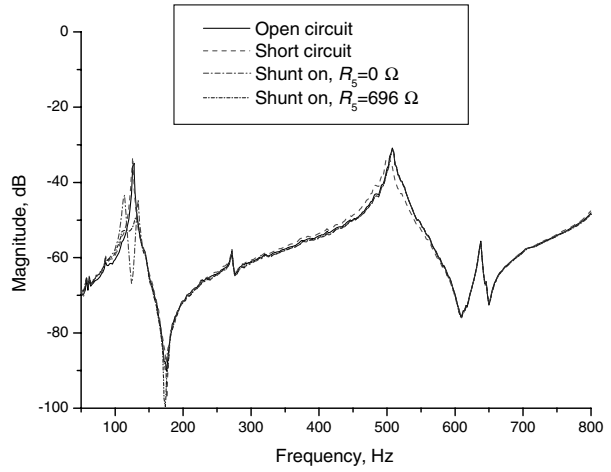

a) Mode (1, 1)

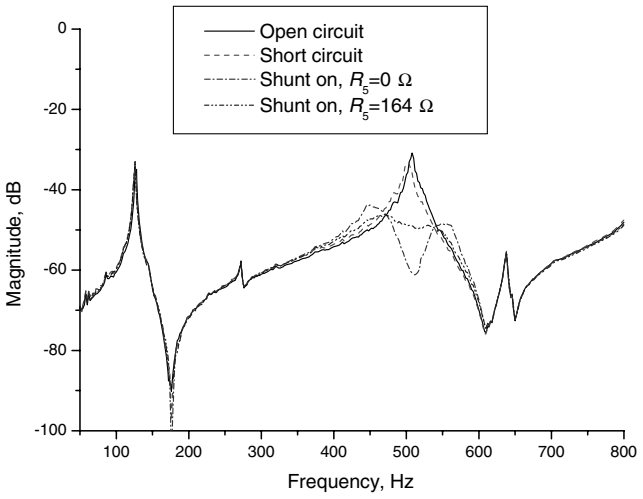

b) Mode (1, 3) + Mode (3, 1)

Fig. 14 Shunt damping effects of initial model.

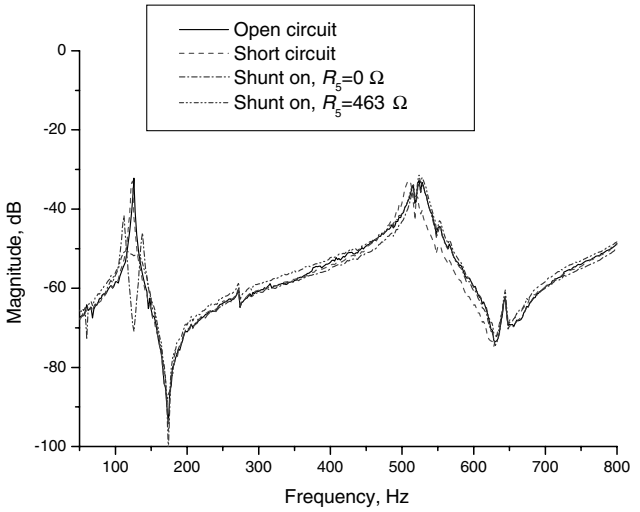

a) Mode (1, 1)

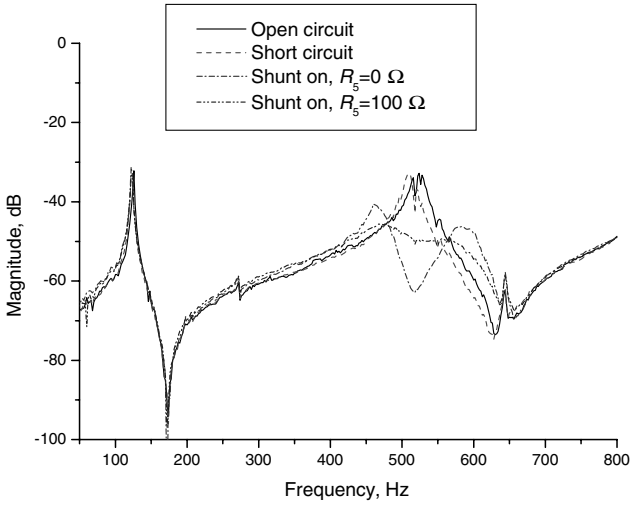

b) Mode (1, 3) + Mode (3, 1)

Fig. 15 Shunt damping effects of optimal model.

$$TL = MNR + 10\log 10(A/S\alpha) \tag{15}$$

where TL is the transmission loss of the panel, MNR is the measured noise reduction between the reverberation room and reception chamber, $S\alpha$ is the Sabine absorption of the reception room, and A is the area of the test window. The expression $10\log 10(A/S\alpha)$ is constant for any test panel with the same area. Therefore, it can be replaced with a constant correction factor CF.

$$TL = MNR - CF \tag{16}$$

To determine this correction factor for the test window, a flexible test panel was made out of 1-mm-thick barrier material to clamp into the test window to calibrate the environment noise level. The transmission loss of the barrier material from 1–1250 Hz can be directly calculated from the mass-law equation.

$$TL_{\text{calc}}\ (\text{dB}) = 20\log 10(W) + 20\log 10(f) - 47.2 \tag{17}$$

where TL_{calc} is the theoretical transmission loss, W is the weight density of the panel, and f is the center frequency of the third-octave measurement band.

Just as in the vibration and acoustics test stand, each panel was clamped into the test window by tightening the bolts to a torque of 20 N · m. The first panel tested was used for calibration. The correction factor is then determined for each third-octave band center frequency.

$$CF = MNR - TL_{\text{calc}} \tag{18}$$

The MNR value can be obtained by measuring the sound pressure level in the reverberation room and semi-anechoic reception room under sine sweep wave exciting.

The second panel was the initial model with shunt circuit. The third panel was the optimal model with shunt circuit. The sine sweep wave was used to excite the test panel from 1–1250 Hz. The test results are presented in Fig. 16. From the figure, the transmission loss

Table 4 Comparisons of the piezoelectric shunt performance between initial and optimal model

Mode number	Initial model		Optimal model		Improvement
(1, 1)	125 Hz	−16 dB	122 Hz	−20 dB	25%
(1, 3) + (3, 1)	496 Hz	−18 dB	512 Hz	−22 dB	22%

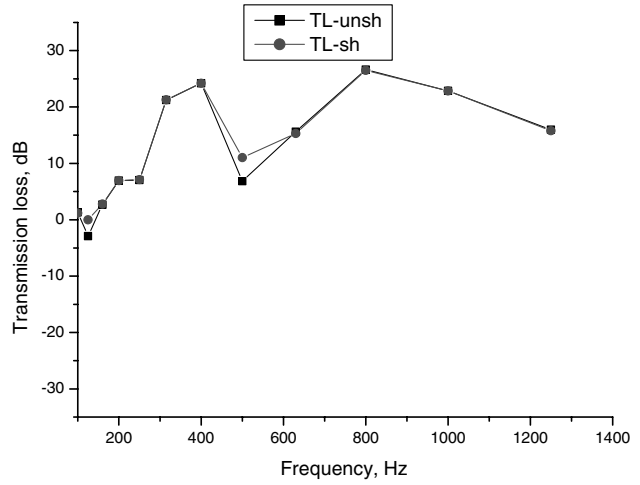

a) Initial model

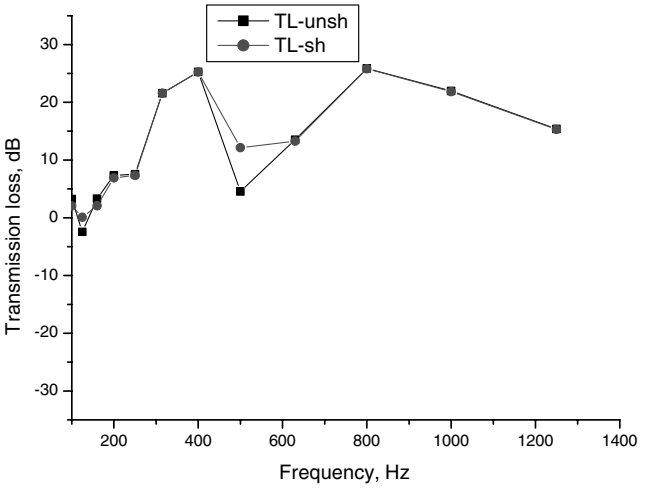

b) Optimal model

Fig. 16 Transmission loss of the initial and optimal model.

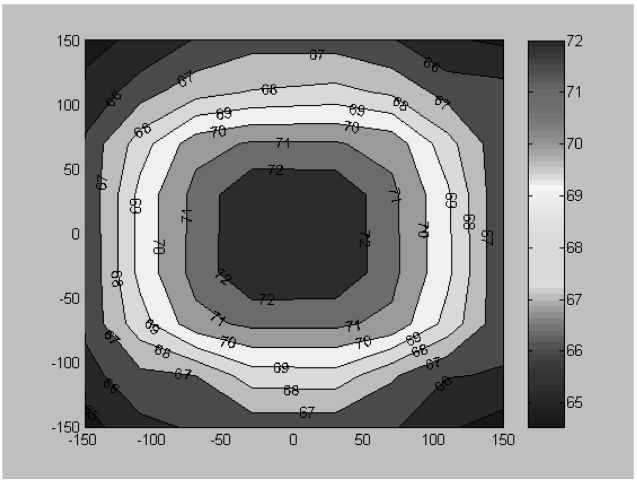

a) Without shunt

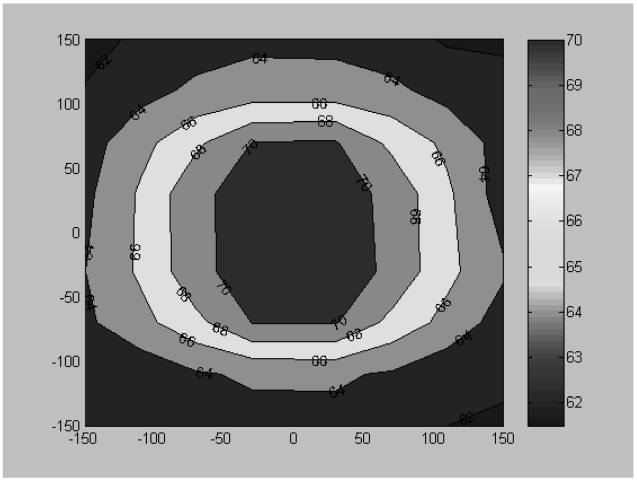

b) With shunt

Fig. 17 Sound pressure distribution of the initial model at mode (1, 3) + mode (3, 1).

of the initial model increased 2 dB for mode (1, 1) and 5 dB for mode (1, 3) + mode (3, 1). However, the transmission loss of the optimal model increased 3 dB for mode (1, 1) and 8 dB for mode (1, 3) + mode (3, 1). As result, the smart panel with shunt circuit switch-on can increase the transmission loss compared to the shunt switch-off. The optimal model can increase 50% at mode (1, 1) and 30% at mode (1, 3) + mode (3, 1) compared to the initial model (Table 5).

D. Sound Pressure Distribution

The sound pressure distribution is studied for visualizing the sound pressure level on the smart panel so as to correlate the mode shapes obtained from the finite element code and shunt damping performance when switching on/off the shunt circuit. Making use of the same setup in the transmission loss test, the 64 points were selected to arrange the locations of microphones. Exciting the smart panel at different resonances with and without shunt, sound pressure distributions are observed in Figs. 17 and 18. From the figures, the contour plots about the sound pressure distribution for the initial model and optimal model are analogous to the mode shapes shown in Fig. 5 and the sound pressure is reduced when the shunt circuit is on. From the sound pressure values, the optimal model can reduce more noise (3 dB) than the initial model (2 dB).

Table 5 Comparison of transmission loss between initial and optimal mode

Mode number	Initial model	Optimal model	Improvement
(1, 1)	−2 dB	−3 dB	50%
(1, 3) + (3, 1)	−5 dB	−8 dB	60%

V. Conclusions

In this paper, admittance is introduced as the performance index of the smart panel. The size, location, and rotation angle of the piezoceramic patch are termed as the control factors and the Taguchi method is used to obtain optimal configuration of the smart panel. Admittance is obtained by the finite element method and impedance analyzer. The resonant shunt circuit is networked with the piezoelectric structure and vibration of the smart panel is reduced under optimal tuning. Transmission loss and sound pressure distribution are measured. Two different smart panels were used for comparing the results of numerical analysis and experiments. The standard facility is proposed according to SAE J1400. Four experiments were executed to correlate the numerical results. Following are some important observations obtained from this study.

1) The optimal configuration of the smart panel was obtained using admittance.

2) The numerical and experimental admittances showed good correlation.

3) The improved shunt performance was observed by comparing the vibration reduction of the initial and optimal model. Using optimal configuration, the performance of the piezoelectric shunt was improved 25% in mode (1, 1) and 22% in mode (1, 3) + mode (3, 1) compared with the initial configuration, respectively.

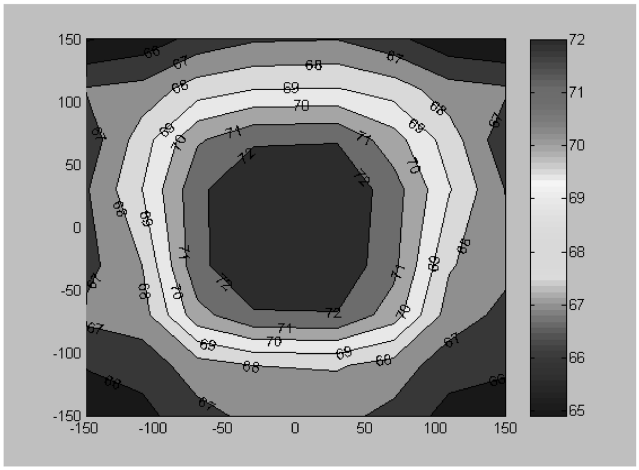

a) Without shunt

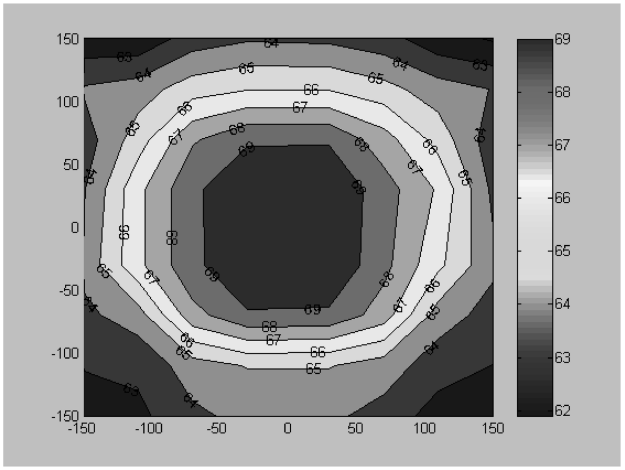

b) With shunt

Fig. 18 Sound pressure distribution of the optimal model at mode (1, 3) + mode (3, 1).

4) Compared with the initial model, transmission loss of the optimal model was increased 50% for mode (1, 1) and 30% for mode (1, 3) + mode (3, 1), respectively.

5) Sound pressure distributions were analogous to mode shapes of the smart panel and sound reduction was observed at the radiating frequencies.

It is expected that the configuration of the smart panel with shunt circuit can be designed using the proposed design procedure.

Acknowledgment

This work was supported by the Inha University Research Grant.

References

[1] Crawley, E. F., "Intelligent Structures for Aerospace: A Technology Overview and Assessment," *AIAA Journal*, Vol. 32, No. 8, 1994, pp. 1689–1699.

[2] Chopra, I., "Review of State-of-Art of Smart Structures and Integrated Systems," *AIAA Journal*, Vol. 40, No. 11, 2002, pp. 2145–2187.

[3] Kim, J., and Lee, J. K., "Broadband Transmission Noise Reduction of Smart Panels Featuring Piezoelectric Shunt Circuits and Sound Absorbing Material," *Journal of the Acoustical Society of America*, Vol. 112, No. 3, 2002, pp. 990–998.

[4] Sun, J. Q., Norris, M. A., Rossetti, D. J., and Highfill, J. H., "Distributed Piezoelectric Actuators for Shell Interior Noise," *Journal of Vibration and Acoustics*, Vol. 118, No. 4, 1996, pp. 676–681.

[5] Shields, W., Ro, J., and Baz, A., "Control of Sound Radiation from a Plate into an Acoustic Cavity Using Active Piezoelectric-Damping Composites," *Proceedings of SPIE: The International Society for Optical Engineering*, Vol. 3039, International Society for Optical Engineering, Bellingham, WA, 1997, pp. 70–90.

[6] Varadan, V. V., Wu, Z., Hong, S. Y., and Varadan, V. K., "Active Control of Sound Radiation from a Vibrating Structure," *IEEE 1991 Ultrasonics Symposium Proceedings*, Vol. 1386, 1991, pp. 991–994.

[7] Varadan, V. V., Gopinathan, S. V., Young, H. L., and Varadan, V. K., "Radiated Noise Control via Structural Vibration Control," *Proceedings of SPIE: The International Society for Optical Engineering*, Vol. 3323, International Society for Optical Engineering, Bellingham, WA, 1998, pp. 546–553.

[8] Lecce, L., Franco, F., Maja, B., Montouri, G., and Zandonella, N. C., "Vibration Active Control Inside a Car by Using Piezo Actuators and Sensors," *28th International Symposium on Automotive Technology and Automation*, 1995, pp. 423–432.

[9] Lee, J. K., Kim, J., Rhee, C. J., Jo, C. H., and Choi, S. B., "Noise Reduction of Passive and Active Hybrid Panels," *Smart Materials and Structures*, Vol. 11, No. 6, 2002, pp. 940–946.

[10] Hagood, N. W., and Flotow, A., "Damping of Structural Vibrations with Piezoelectric Materials and Passive Electrical Networks," *Journal of Sound and Vibration*, Vol. 146, No. 2, 1991, pp. 243–268.

[11] Law, H. H., Rossiter, P. L., Simon, G. P., and Koss, L. L., "Characterization of Mechanical Vibration Damping by Piezoelectric Materials," *Journal of Sound and Vibration*, Vol. 197, No. 4, 1996, pp. 489–513.

[12] Moheimani, S.O.R., "Survey of Recent Innovations in Vibration Damping and Control Using Shunted Piezoelectric Transducers," *IEEE Transactions on Control Systems Technology*, Vol. 11, No. 4, 2003, pp. 482–494.

[13] Lesieutre, G. A., "Vibration Damping and Control Using Shunted Piezoelectric Materials," *The Shock and Vibration Digest*, Vol. 30, No. 3, 1998, pp. 187–195.

[14] Wu, S. Y., "Method for Multiple Mode Shunt Damping of Structural Vibration Using Single PZT Transducer," *Proceedings of SPIE: The International Society for Optical Engineering*, Vol. 3327, International Society for Optical Engineering, Bellingham, WA, 1998, pp. 159–168.

[15] Behrens, S., Fleming, A. J., and Moheimani, S. O. R., "New Method for Multiple-Mode Shunt Damping of Structural Vibration Using Single Piezoelectric Transducer," *Proceedings of SPIE: The International Society for Optical Engineering*, Vol. 4331, International Society for Optical Engineering, Bellingham, WA, 2001, pp. 239–250.

[16] Kim, J., Ryu, Y. H., and Choi, S. B., "New Shunting Parameter Tuning Method for Piezoelectric Damping Based on Measured Electrical Impedance," *Smart Materials and Structures*, Vol. 9, No. 6, 2000, pp. 868–877.

[17] Tsai, M. S., and Wang, K. W., "Some Insight on Active-Passive Hybrid Piezoelectric Networks for Structural Controls," *Proceedings of SPIE: The International Society for Optical Engineering*, Vol. 3045, International Society for Optical Engineering, Bellingham, WA, 1997, pp. 82–93.

[18] Tsai, M. S., and Wang, K. W., "On The Structural Damping Characteristics of Active Piezoelectric Actuators with Passive Shunt," *Journal of Sound and Vibration*, Vol. 221, No. 1, 1999, pp. 1–22.

[19] Zhang, J. M., Chang, W., Varadan, V. K., and Varadan, V. V., "Passive Underwater Acoustic Damping Using Shunted Piezoelectric Coatings," *Smart Materials and Structures*, Vol. 10, No. 2, 2000, pp. 414–420.

[20] Kim, J., and Lee, J. K., "Broadband Transmission Noise Reduction of Smart Panels Featuring Piezoelectric Shunt Circuits and Sound Absorbing Material," *Journal of the Acoustical Society of America*, Vol. 112, No. 3, 2002, pp. 990–998.

[21] Bianchini, E., Spangler, R., and Pandell, T., "Use of Piezoelectric Dampers for Improving the Fell of Golf Clubs," *Proceedings of SPIE: The International Society for Optical Engineering*, Vol. 3688, International Society for Optical Engineering, Bellingham, WA, 1999, pp. 824–834.

[22] Bianchini, E., and Spangler, R., "Use of Piezoelectric Devices to Control Snowboard Vibrations," *Proceedings of SPIE: The International Society for Optical Engineering*, Vol. 3329, International Society for Optical Engineering, Bellingham, WA, 1998, pp. 106–114.

[23] Park, J. S., Lim, S. C., Choi, S. B., Kim, J. H., and Park, Y. P., "Vibration Reduction of a CD-ROM Drive Base Using a Piezoelectric Shunt Circuit," *Journal of Sound and Vibration*, Vol. 269, No. 3, 2004, pp. 1111–1118.

[24] Liang, C., Sun, F. P., and Rogers, C. A., "Electro-Mechanical Impedance Modeling of Active Material Systems," *Smart Materials and Structures*, Vol. 5, No. 11, 1996, pp. 171–186.

[25] Kim, J., and Kim, J. H., "Multimode Shunt Damping of Piezoelectric Smart Panel for Noise Reduction," *Journal of the Acoustical Society of America*, Vol. 116, No. 2, 2004, pp. 942–948.

[26] Rizzoni, G., *Principles and Applications of Electrical Engineering*, 2nd ed., McGraw–Hill, New York, 1996.
[27] Powell, D. J., Mould, J., and Wojcik, G. L., "Dielectric and Mechanical Absorption Mechanisms for Time Frequency Domain Transducer Modeling," *IEEE Ultrasonic Symposium Proceedings*, Vol. 2, 1998, pp. 1019–1024.
[28] Kim, J., Varadan, V. V., Varadan, V. K., and Bao, X. Q., "Finite-Element Modeling of a Smart Cantilever Plate and Comparison with Experiments," *Smart Materials and Structures*, Vol. 5, No. 12, 1996, pp. 165–170.
[29] Varadan, V. V., Lim, Y. H., and Varadan, V. K., "Closed Loop Finite-Element Modeling of Active/Passive Damping in Structural Vibration Control," *Smart Materials and Structures*, Vol. 5, No. 9, 1996, pp. 685–694.
[30] "ANSYS Theory Manual," Ver. 5.5, ANSYS, SAS IP, 1999.
[31] Ross, P. J., *Taguchi Techniques for Quality Engineering*, 2nd ed., Mcgraw–Hill, New York, 1996.
[32] Ahmadian, M., and Jeric, K. M., "On the Application of Shunted Piezoceramics for Increasing Acoustic Transmission Loss in Structures," *Journal of Sound and Vibration*, Vol. 243, No. 2, 2001, pp. 347–359.

E. Livne
Associate Editor